

Cooperative emission in quantum plasmonic superradiance

H. Varguet, S. Guérin, H. Jauslin, and G. Colas des Francs*

 Laboratoire Interdisciplinaire Carnot de Bourgogne (ICB), UMR 6303 CNRS, Université Bourgogne Franche-Comté,
 9 Avenue Savary, Boîte Postale 47870, 21078 Dijon Cedex, France

 (Received 19 October 2018; revised manuscript received 11 April 2019; published 29 July 2019)

Plasmonic superradiance originates from the plasmon mediated strong correlation that builds up between dipolar emitters coupled to a metal nanoparticle. This leads to a fast burst of emission so that plasmonic superradiance constitutes ultrafast and extremely bright optical nanosources of strong interest for integrated quantum nano-optics platforms. We elucidate the superradiance effect by establishing the dynamics of the system, including all features such as the orientation of the dipoles, their distance to the particle, and the number of active plasmon modes. We determine an optimal configuration for Purcell enhanced superradiance. We also show superradiance blockade at small distances.

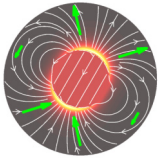
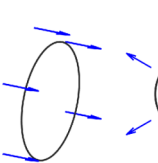
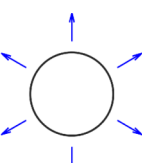
 DOI: [10.1103/PhysRevB.100.041115](https://doi.org/10.1103/PhysRevB.100.041115)

Introduction. In a seminal work, Dicke discovered that a set of N_e atoms radiate collectively when they occupy a subwavelength volume. Their emission is much faster ($\tau_{N_e} = \tau_1/N_e$) and stronger ($I_{N_e} = N_e^2 I_1$) than for independent atoms. This so-called superradiance originates from spontaneous phase locking of the atomic dipoles through a same mode and is very similar to the building of cooperative emission in a laser amplifier [1]. Superradiant emission produces original states of light with applications such as narrow linewidth lasers [2] or quantum memories [3,4]. Single collective excitation of atoms in a nanofiber has been demonstrated [5] and superradiantlike behavior was suggested in a plasmonics junction [6] or a nanocrystal [7], pushing further integration capabilities of quantum technologies. Putsovit and Shahbazyan identified plasmon enhanced collective emission for dipoles coupled to a metal nanoparticle (MNP) [8], considering a classical approach which, however, cannot describe the Dicke cascade at the origin of the cooperative emission. In this Rapid Communication, taking benefit from recent advances on quantum plasmonics and open quantum systems [9–17], we derive a quantum approach for plasmonic superradiance and discuss the dynamics of cooperative emission with particular attention to the role of the localized surface plasmons (LSP $_n$, where n refers to the mode order).

Single excitation superradiance. We first consider single excitation superradiance that presents a classical analog, facilitating the physical representation of the collective process. It reduces to an eigenvalue problem on the dipole moment $\vec{d}^{(i)}$ of N_e emitters located at \vec{r}_i [8,18–21]:

$$\left[\left(i \frac{\Gamma_{\text{tot}}}{2} + \Delta_{\text{tot}} \right) \mathbb{1} - \frac{3}{2k_0^3} \Gamma_0 \sum_{j=1}^{N_e} \mathbf{G}(\vec{r}_j, \vec{r}_i, \omega_0) \right] \cdot \vec{d}^{(i)} = 0, \quad (1)$$

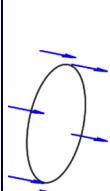
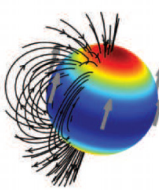
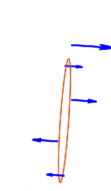
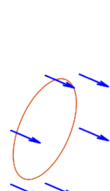
TABLE I. Bright states with six emitters at 20 nm from a 30 nm MNP ($\omega_0 = 2.77$ eV). The field lines of LSP $_1$ are superimposed to the brightest configuration.

			
$\Gamma_{\text{tot}}/\Gamma_0$	325	93	2.7
$\Gamma_{\text{tot}}/\Gamma_1$	-	5.74	0.03

where \mathbf{G} is the Green's tensor in the presence of the MNP, ω_0 is the angular frequency of emission, and $k_0 = \omega_0/c$. Γ_0 is the free-space dipolar decay rate. We assume a Drude behavior $\varepsilon_m(\omega) = \varepsilon_\infty - \omega_p^2/(\omega^2 + i\gamma_p\omega)$ with $\varepsilon_\infty = 6$, $\hbar\omega_p = 7.90$ eV, and $\hbar\gamma_p = 51$ meV for silver.

Typical plasmonic collective states (eigenmodes) are presented in Table I. The brightest state ($\Gamma_{\text{tot}}/\Gamma_0 = 325$) is obtained for dipoles that are parallel to the field lines of LSP $_1$, which favors the collective coupling, and most of them (four

TABLE II. Brightest states maximizing $\Gamma_{\text{tot}}/\Gamma_1$ and considering single mode MNP response. The field lines are indicated for LSP $_1$. Γ_1 refers to single emitter configuration (all LSPs or single mode).

				
$\Gamma_{\text{tot}}/\Gamma_1$	5.74	6	3	2.25

*gerard.colas-des-francs@u-bourgogne.fr

out of six) are almost perpendicular to the MNP surface, corresponding to a strongly enhanced decay rate. We also observe simple configurations maximizing the ratio $\Gamma_{\text{tot}}/\Gamma_1$ where Γ_1 refers to a single emitter (azimuthal or radial) coupled to the MNP. For azimuthal emitters $\Gamma_{\text{tot}}/\Gamma_1 = 5.74$, but for radial orientation, $\Gamma_{\text{tot}}/\Gamma_1 = 0.03$ only. In Table II, we show the role of LSPs for the azimuthal ring arrangement. It presents an ideal superradiant behavior ($\Gamma_{\text{tot}}^1 = N_e \Gamma_1^1$) when LSP₁ is the only mode involved since all the emitters couple equivalently to LSP₁, as displayed by the field lines. This arrangement is also a bright state for LSP₃ but not for LSP₂ where the dipoles oscillate out of phase. Although the single excitation superradiance can be understood from quantum or classical approaches, only a quantum approach is able to describe the dynamics of the preparation of coherent superradiant states.

Quantum master equation. The dynamics of N_e emitters coupled to a MNP is governed by an effective Hamiltonian, involving the transition operators $\hat{\sigma}_{\pm}^{(i)}$ of the emitter i , the bosonic operators associated to LSPs [22], and fully taking into account the emitter's and LSP's losses [23]. In the weak-coupling regime, the LSPs are practically not populated due to their strong dissipation. The adiabatic elimination therefore permits one to transfer the information on the LSPs losses to the effective dynamics of the excited emitters. We obtain the Lindblad master equation for the density operator $\hat{\rho}$ of the emitters [24]:

$$\frac{d\hat{\rho}(t)}{dt} = \sum_{j=1}^{N_e} \sum_{k=1}^{N_e} \frac{1}{i\hbar} [\hat{H}_{jk}, \hat{\rho}(t)] + \mathcal{D}_{jk}[\hat{\rho}(t)], \quad (2)$$

with

$$\hat{H}_{jk} = -\hbar \Delta_{jk} \hat{\sigma}_{+}^{(k)} \hat{\sigma}_{-}^{(j)}, \quad (3a)$$

$$\mathcal{D}_{jk}[\hat{\rho}(t)] = \Gamma_{jk} [\hat{\sigma}_{-}^{(j)} \hat{\rho}(t) \hat{\sigma}_{+}^{(k)} - \frac{1}{2} (\hat{\sigma}_{+}^{(k)} \hat{\sigma}_{-}^{(j)} \hat{\rho}(t) + \hat{\rho}(t) \hat{\sigma}_{+}^{(k)} \hat{\sigma}_{-}^{(j)})]. \quad (3b)$$

The parameter $\Gamma_j = \Gamma_{jj}$ ($\Delta_j = \Delta_{jj}$) represents the decay rate (Lamb shift) of the emitter j in the presence of the MNP. For $j \neq k$, Γ_{jk} and Δ_{jk} characterize the cooperative decay rate and population transfer. In particular,

$$\Gamma_{jk} = \sum_{n=1}^{N_e} \frac{\gamma_n}{\delta_n^2 + (\frac{\gamma_n}{2})^2} g_n^{(j)} g_n^{(k)} \mu_n^{(jk)}, \quad (4)$$

where we introduced the coupling strength $g_n^{(j)}$ between the emitter j and the mode LSP _{n} . $\mu_n^{(jk)}$ is the coupling strength between emitters i and j via LSP _{n} [24]. This plays an important role in the emitters' dynamics since, depending on its sign, it can lead to either enhancement or blockade of the cooperative process.

Cooperative emission. In the case of plasmonic Dicke states, the coupling to LSPs strongly depends on the emitter orientation and the number of active LSP modes. We work in the basis $\{|ee \dots ee\rangle, \mathcal{P}_{N_e}^{N_e-1}(|\alpha\rangle), \dots, \mathcal{P}_{N_e}^1(|\alpha\rangle), |gg \dots gg\rangle\}$, where the permutator $\mathcal{P}_{N_e}^{N_e-l}(|\alpha\rangle)$ gives all the states $|\alpha\rangle$ with $N_e - l$ excited emitters. For instance, $\mathcal{P}_3^2(|\alpha\rangle) = \{|eeg\rangle, |ege\rangle, |gee\rangle\}$. The collective emission can be written as

$I(t) = \hbar\omega_0 W(t)$ with the collective rate

$$W(t) = \left\langle \sum_{i,j=1}^{N_e} \Gamma_{ij} \hat{\sigma}_{+}^{(i)} \hat{\sigma}_{-}^{(j)} \right\rangle = \text{Tr} \left(\hat{\rho} \sum_{i,j} \Gamma_{ij} \hat{\sigma}_{+}^{(i)} \hat{\sigma}_{-}^{(j)} \right). \quad (5)$$

This expression generalizes the standard definition to the case of nonequal rates Γ_{ij} . It can be separated into two contributions: W_P involving the populations and W_C involving coherences. For instance, in the presence of two emitters:

$$W_P(t) = (\Gamma_1 + \Gamma_2) \langle ee | \hat{\rho}(t) | ee \rangle + \Gamma_1 \langle eg | \hat{\rho}(t) | eg \rangle + \Gamma_2 \langle ge | \hat{\rho}(t) | ge \rangle, \quad (6a)$$

$$W_C(t) = \Gamma_{12} [\langle ge | \hat{\rho}(t) | eg \rangle + \langle eg | \hat{\rho}(t) | ge \rangle]. \quad (6b)$$

Similar expressions can be derived for an arbitrary number of emitters. For independent emitters ($\mu_{i \neq j} = 0$), the decay rates Γ_{ij} cancel for $i \neq j$. The emission rate reduces to incoherent emission W_P of the independent emitters. The second term W_C describes the collective behavior of the ensemble of emitters when $\mu_{ij} \neq 0$. Therefore, the cooperative behavior originates from the correlation between the states of same excitation $\mathcal{P}_{N_e}^{N_e-l}(|\alpha\rangle)$ in full analogy with free-space superradiance.

Finally, we emphasize that the collective rate $W(t)$ includes both radiation in the far field and nonradiative transfer to the absorbing MNP. Since the cooperative decay rate can be written equivalently as $\Gamma_{jk} = 2\omega_0^2 / (\hbar\epsilon_0 c^2) \text{Im}[\mathbf{d}^{(j)} \cdot \mathbf{G}(\mathbf{r}_j, \mathbf{r}_k, \omega_0) \cdot \mathbf{d}^{(k)}]$ [24], one can isolate the radiative rates Γ_{ij}^{rad} in the quasistatic approximation [8], and the far-field radiated emission obeys $I_{\text{rad}}(t) = \hbar\omega_0 W_{\text{rad}}(t)$ with

$$W_{\text{rad}}(t) = \left\langle \sum_{i,j=1}^{N_e} \Gamma_{ij}^{\text{rad}} \hat{\sigma}_{+}^{(i)} \hat{\sigma}_{-}^{(j)} \right\rangle. \quad (7)$$

The master equation (2) is solved numerically following Refs. [30,31] assuming the initial state $|\psi(0)\rangle = |e \dots e\rangle$. Figure 1 represents the dynamics of correlated emission. We consider three configurations (black lines): azimuthal emitters (perpendicular to the equator) at distance $h = 20$ nm in Fig. 1(a) and radial emitters at $h = 20$ nm [Fig. 1(b)], or $h = 2$ nm [Fig. 1(c)], and their comparison with two limit cases: ideal superradiance (emitters at the same position, red lines) and incoherent emission (W_P , blue lines). In the case of azimuthal orientation and for $h = 20$ nm [Fig. 1(a)], all the emitters equally couple to LSP₁ so that close to ideal superradiance is observed for both total and radiative emissions with a collective quantum yield $\eta = W_{\text{rad}}/W = 1/15.3 = 7\%$. For radial emitters, we still observe the burst of emission but less pronounced [Fig. 1(b)]. At short distances [$h = 2$ nm; Fig. 1(c)], almost incoherent emission occurs. The cooperative behavior is partially recovered for 20 nm ($\eta = 13\%$) and $h = 2$ nm ($\eta = 5\%$) if the emitters are at the poles [green curves in Figs. 1(b) and 1(c)], a configuration achievable by nanoscale photopolymerization [32].

Plasmonic Dicke states (ideal superradiance). When all the emitters are located at the same position, $\Gamma_{ij} = \Gamma_1$, $\Delta_{ij} = \Delta_1$ so that we can work with the Dicke ladder ($J = N_e/2$)

$$|J, M\rangle = \sqrt{\frac{(J+M)!}{N_e!(J-M)!}} \hat{J}_-^{J-M} |ee \dots e\rangle, \quad (8)$$

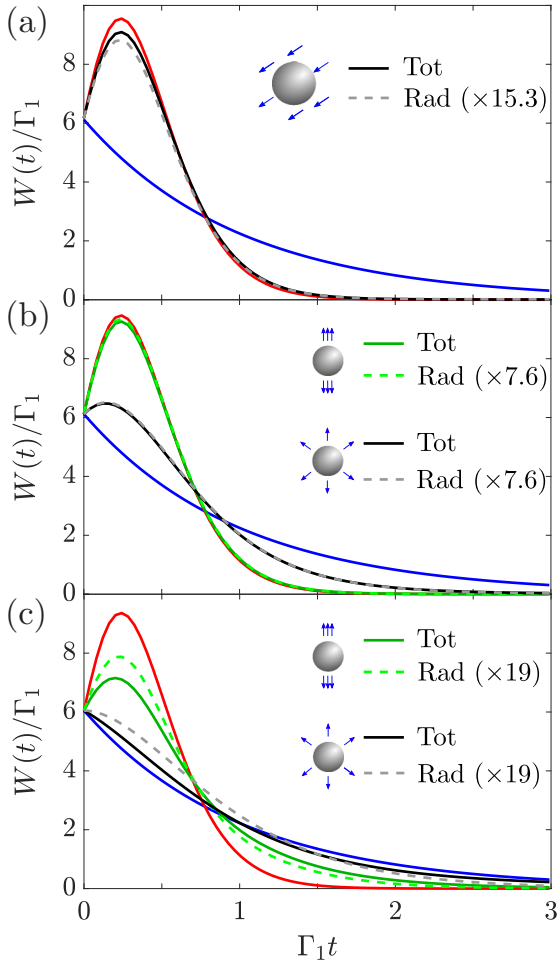


FIG. 1. Normalized collective rate $W(t)/\Gamma_1$ for six emitters ($\omega_0 = \omega_1 = 2.77$ eV). (a) Azimuthal orientation, $h = 20$ nm; (b) radial orientation, $h = 20$ nm; (c) radial, $h = 2$ nm. Red curves: ideal superradiance; blue curves: incoherent emission. Green and black curves correspond to emitters at the poles or homogeneously distributed, respectively. Dashed lines refer to the radiative collective rate W_{rad} .

where we have introduced the collective spin operator $\hat{J}_{\pm} = \sum_{i=1}^{N_e} \hat{\sigma}_{\pm}^{(i)}$. The state $|J, J\rangle = |ee \dots e\rangle$ has all the emitters in their excited state and the symmetrized Dicke state $|J, M\rangle$ is a superposition of the states with $J + M$ excited emitters. The master equation (2) simplifies to

$$\frac{d\rho_M(t)}{dt} = \Gamma_{M+1}\rho_{M+1}(t) - \Gamma_M\rho_M(t),$$

where $\rho_M(t) = \langle J, M | \hat{\rho}(t) | J, M \rangle$ and $\Gamma_M = (J + M)(J - M + 1)\Gamma_1$ are the population and the collective rate of the state $|J, M\rangle$, respectively. The dynamics is the exact analog of free-space superradiance except that the decay rate is replaced by its value in the presence of the MNP, and superradiance is enhanced by the Purcell factor Γ_1/Γ_0 . Finally, the plasmonic superradiance originates from the cascade along the Dicke states ladder. Beginning with the initial condition $|\psi(t=0)\rangle = |ee \dots e\rangle = |J, J\rangle$, the system successively goes through the Dicke states $|J, M\rangle$ with $M = J - 1, J - 2, \dots$, down to the final ground state $|J, -J\rangle = |gg \dots g\rangle$. The decay

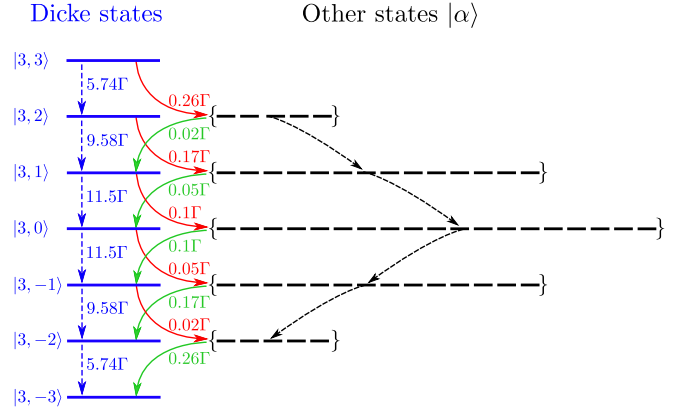


FIG. 2. Superradiance cascade along extended Dicke basis for six azimuthal emitters homogeneously distributed [same as black curve in Fig. 1(a)].

rate starts from $\Gamma_M = N_e\Gamma_1$ for $M = J$, increases up to $\Gamma_M \approx N_e^2\Gamma_1$ for $M = 0, \pm 1/2$ (depending on the parity of J), and then decreases down to $\Gamma_M = 0$ for the final ground state. The buildup of this cooperative behavior is shown in Fig. 1 (red curves). Since the direct dipole-dipole coupling is negligible compared to the LSP mediated dipole-dipole coupling, we avoid the van der Waals dephasing observed for free-space configurations [1].

Extended Dicke basis. Moving away from the ideal configuration, it is necessary to generalize the superradiance ladder to describe the full dynamics [33]. In the case of small deviation from ideal superradiance, it is worth working in an extended Dicke basis including the Dicke states. The decay rates along the Dicke ladder are calculated from the expression $\Gamma_{M \rightarrow M'} = \langle \tilde{M} | \mathcal{D}_{[\rho]} | \tilde{M} \rangle$ where $|\tilde{M}\rangle$ is the vector representation of the projector $|J, M\rangle\langle J, M|$ on the Dicke states and $\mathcal{D}_{[\rho]}$ is the associated representation of the dissipator \mathcal{D} [24,31]. The parasitic transitions to all other states $|\alpha\rangle$ follows $\gamma_{M \rightarrow \alpha} = \Gamma_M - \Gamma_{M \rightarrow M'}$ where $\Gamma_M = \langle J, M | \sum_{i,j=1}^{N_e} \Gamma_{ij} \hat{\sigma}_+^{(i)} \hat{\sigma}_-^{(j)} | J, M \rangle$ is the decay rate of the Dicke state $|J, M\rangle$. Similar formulas are used to estimate the input rates $\gamma_{\alpha \rightarrow M'}$ from states $|\alpha\rangle$. Namely, $\gamma_{\alpha \rightarrow M'} = \langle J, M' | \sum_{i,j=1}^{N_e} \Gamma_{ij} \hat{\sigma}_-^{(i)} \hat{\sigma}_+^{(j)} | J, M' \rangle - \Gamma_{M \rightarrow M'}$. Figure 2 presents the superradiance cascade along the extended Dicke basis. The decay rates along the Dicke ladder ($\Gamma/\Gamma_1 : 5.75 \rightarrow 9.58 \rightarrow 11.5 \rightarrow 11.5 \rightarrow 9.58 \rightarrow 5.75$) closely follow the ideal values ($\Gamma/\Gamma_1 : 6 \rightarrow 10 \rightarrow 12 \rightarrow 12 \rightarrow 10 \rightarrow 6$) for azimuthal emitters so that one still observes a burst of emission in Fig. 1(a) (black solid line). Parasitic transitions outside the Dicke ladder slightly degrade the collective emission.

Role of LSPs. We discuss the role of LSPs on the superradiance emission considering two emitters located at the same distance to the MNP (but not the same position). We work in the Dicke basis $|ee\rangle, |S\rangle, |A\rangle, |gg\rangle$ with the symmetric and antisymmetric states

$$|S\rangle = \frac{1}{\sqrt{2}}(|ge\rangle + |eg\rangle), \quad |A\rangle = \frac{1}{\sqrt{2}}(|ge\rangle - |eg\rangle). \quad (9)$$

Their populations dynamics are given by

$$\partial_t \rho_{ee}(t) = -2\Gamma_1 \rho_{ee}(t), \quad (10a)$$

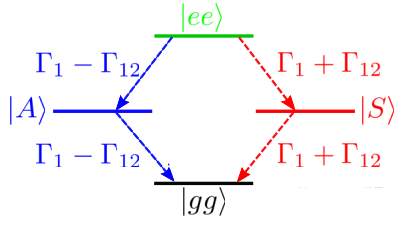


FIG. 3. Dicke ladder for two emitters-MNP configuration.

$$\partial_t \rho_{S,A}(t) = \Gamma_{S,A} \rho_{ee}(t) - \Gamma_{S,A} \rho_{S,A}(t), \quad (10b)$$

$$\partial_t \rho_{gg}(t) = \Gamma_S \rho_S(t) + \Gamma_A \rho_A(t), \quad (10c)$$

as displayed in Fig. 3. The population of the excited state $|ee\rangle$ decays exponentially with the rate $\Gamma_{ee} = 2\Gamma_1$ that does not depend on the angle between the emitters. The symmetric and antisymmetric states are populated from $|ee\rangle$ with the rates

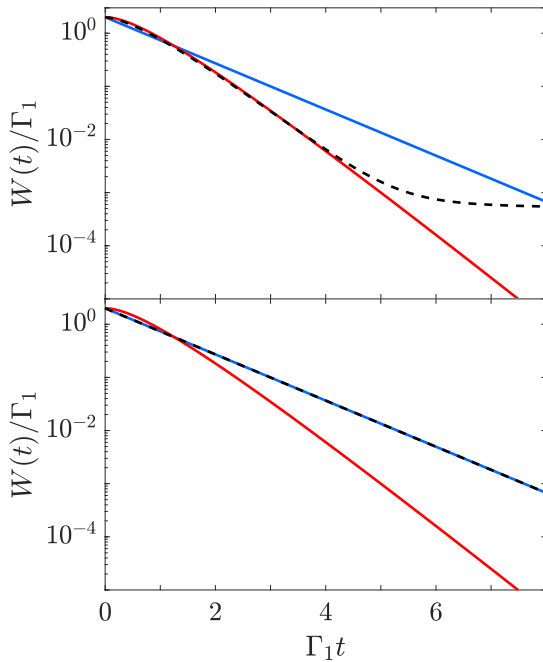
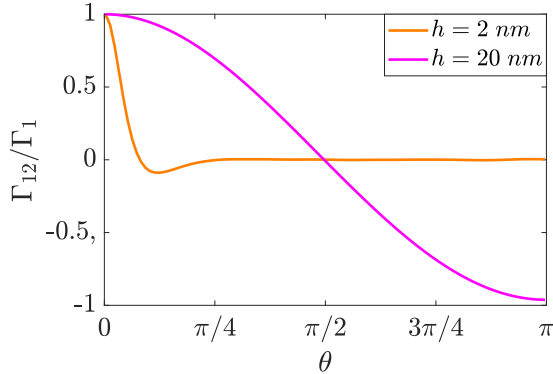


FIG. 4. (a) Two emitters cooperative decay rate Γ_{12} as a function of their angular separation θ , for two distances $h = 2$ or 20 nm. (b),(c) Collective rate $W(t)$ for two emitters. (b) $h = 20$ nm ($\omega_0 = 2.771$ eV) and (c) $h = 2$ nm ($\omega_0 = 2.964$ eV). In (b) and (c), red curves correspond to ideal superradiance, blue curves to incoherent emission, and black curves to the emitter located at the poles.

TABLE III. Plasmonic super/subradiant states with two emitters ($h = 20$ nm, $\omega_0 = 2.771$ eV). The decay rate is normalized with respect to a single emitter decay rate for the same configuration (radial or azimuthal).

$\frac{\Gamma_2}{\Gamma_1}$	1.96	1.92	0.08	0.04

$\Gamma_{S,A} = (\Gamma_1 \pm \Gamma_{12})$ and relax toward the ground state with the same rates. Finally, the collective decay rate is

$$W(t) = 2\Gamma_1 \rho_{ee}(t) + \Gamma_S \rho_S(t) + \Gamma_A \rho_A(t). \quad (11)$$

The cooperative relaxation strongly depends on Γ_{12} , and thus on the emitter's positions. Figure 4(a) shows the cooperative rate $\Gamma_{12}(\theta)$. For two emitters at the same position, $\Gamma_{12}(0) = \Gamma_1$, and we recover the ideal superradiant configuration. The bright superradiant state $|S\rangle$ decays with the rate $\Gamma_S = N_e \Gamma_1$ ($N_e = 2$) and the dark subradiant state is $|A\rangle$, which is not populated and presents a zero decay rate $\Gamma_A = 0$. For emitters located at the poles ($\theta = \pi$) the collective behavior depends on the distance to the MNP. For large separation distances, only the dipolar LSP₁ mode significantly contributes to the emitters-MNP coupling and $\Gamma_{12}(\pi) \approx -\Gamma_1$. Superradiant and subradiant states are exchanged ($|A\rangle$ and $|S\rangle$, respectively), but the collective dynamics [black curve, Fig. 4(b)] is close to the ideal case. At smaller distances, the cooperative behavior is inhibited ($\Gamma_{12} \approx 0$) in the presence of high-order LSPs because of destructive superposition of their contribution [11,22]. This results in a superradiance blockade and the dynamics closely follows an incoherent process [Fig. 4(c)].

The superradiance blockade can be also inferred from the eigenvalue model [Eq. (1)]. The eigenvectors are represented in Table III. We check that $\Gamma_S + \Gamma_A = 2\Gamma_1$ for all symmetric/antisymmetric pairs in agreement with Fig. 3. However, for small separation distance $h = 2$ nm and $\omega_0 = 2.964$ eV, corresponding to high-order modes resonance, the cooperative rate vanishes for both radial and azimuthal emitters and the dynamics is almost incoherent. In order to understand this behavior more deeply, we consider each mode

TABLE IV. Plasmonic bright states considering single mode MNP response (LSP_n) and two radial emitters ($h = 2$ nm, $\omega_0 = 2.964$ eV). The mode field lines and charge density are indicated.

LSP _n	n=1	n=2	n=3

separately in Table IV. The alternating charge distribution at the position of the dipole clearly leads to cancellation of the cooperative behavior by destructive interferences. This corresponds to a coupling strength between the two emitters $\mu_{\text{odd}}^{12} \approx 1$, $\mu_{\text{even}}^{12} \approx -1$. Therefore, the quantum collective decay rate Γ_{12} vanishes at short distances when numerous LSP modes are involved [Eq. (4)]. It is worth noticing that the collective rate plays a role in the whole quantum superradiance cascade dynamics and not only for the single excitation state, which is the only one considered in the eigenvalue model. This explains the discrepancy between the partial superradiance observed for radial emitters in the quantum approach [with six excitations as the initial state; Fig. 1(b)] and the almost zero decay rate of the single excitation state (see Table I), which is not populated during the superradiance process.

Conclusion and outlook. We have derived a quantum approach for plasmonic superradiance and discussed the dynamics of cooperative emission. The system follows the plasmonic Dicke ladder and strong LSP mediated correlations build up between the emitters so that superradiance can be Purcell enhanced. Since the buildup of the cooperative emission ($\sim 1/N_e \Gamma_1$) has to be smaller than the dephasing rate γ^* [1], this would facilitate the conditions to achieve super-

radiance. However, superradiance blockade occurs at small distances where cooperativity is jeopardized because of modal destructive interferences. Finally, our work brings a deeper understanding of light-matter interaction at the nanoscale which can be helpful in designing a surface plasmon laser (SPASER) since it relies on a very similar mechanism [34]. We considered identical emitters throughout this work and we expect that the superradiance should be degraded for nonidentical emitters. However, some recent works indicate that cooperative dissipation in a nanocrystal could help to recover the superradiance effect [7] and we expect that plasmonic superradiance could be experimentally investigated on metalodielectric nanohybrids [32,35–37]. More generally, our approach opens up the possibility to systematically optimize the superradiance effect for different geometries of the nanoparticles [38].

Acknowledgments. This work is supported by the French “Investissements d’Avenir” program: ISITE-BFC IQUINS (ANR-15-IDEX-03) and EUR-EIPHI (17-EURE-0002). This work is part of the European COST action MP1403 Nanoscale Quantum Optics. Additional support from the European Union’s Horizon 2020 Research and Innovation Program under Marie Skłodowska-Curie Grant Agreement No. 765075 (LIMQUET) is acknowledged.

-
- [1] M. Gross and S. Haroche, *Phys. Rep.* **93**, 301 (1982).
- [2] J. G. Bohnet, Z. Chen, J. M. Weiner, D. Meiser, M. J. Holland, and J. K. Thompson, *Nature (London)* **484**, 78 (2012).
- [3] M. Afzelius, N. Gisin, and H. Riedmatten, *Phys. Today* **68** (12), 42 (2015).
- [4] J. Kim, D. Yang, S.-H. Oh, and K. An, *Science* **359**, 662 (2017).
- [5] N. Corzo, J. Raskop, A. Chandra, A. Sheremet, B. Gouraud, and J. Laurat, *Nature* **566**, 359 (2019).
- [6] H. Groß, J. M. Hamm, T. Tufarelli, O. Hess, and B. Hecht, *Sci. Adv.* **4**, eaar4906 (2018).
- [7] B. Prasanna Venkatesh, M. L. Juan, and O. Romero-Isart, *Phys. Rev. Lett.* **120**, 033602 (2018).
- [8] V. N. Pustovit and T. V. Shahbazyan, *Phys. Rev. Lett.* **102**, 077401 (2009).
- [9] C. Van Vlack, P. T. Kristensen, and S. Hughes, *Phys. Rev. B* **85**, 075303 (2012).
- [10] M. S. Tame, K. R. McEnery, S. K. Ozdemir, J. Lee, S. A. Maier, and M. S. Kim, *Nat. Phys.* **9**, 329 (2013).
- [11] B. Rousseaux, D. Dzsojtjan, G. Colas des Francs, H. R. Jauslin, C. Couteau, and S. Guérin, *Phys. Rev. B* **93**, 045422 (2016); **94**, 199902(E) (2016).
- [12] A. Drezet, *Phys. Rev. A* **95**, 023831 (2017).
- [13] F. Marquier, C. Sauvan, and J.-J. Greffet, *ACS Photonics* **4**, 2091 (2017).
- [14] I. E. Protsenko, A. V. Uskov, X.-W. Chen, and H. Xu, *J. Phys. D: Appl. Phys.* **50**, 2 (2017).
- [15] R. Saez-Blazquez, J. Feist, A. Fernandez-Dominguez, and F. J. Garcia-Vidal, *Optica* **4**, 1363 (2017).
- [16] A. Asenjo-Garcia, J. D. Hood, D. E. Chang, and H. J. Kimble, *Phys. Rev. A* **95**, 033818 (2017).
- [17] N. Yokoshi, K. Odagiri, A. Ishikawa, and H. Ishihara, *Phys. Rev. Lett.* **118**, 203601 (2017).
- [18] M. O. Araujo, I. Krešić, R. Kaiser, and W. Guerin, *Phys. Rev. Lett.* **117**, 073002 (2016).
- [19] J.-J. Choquette, K.-P. Marzlin, and B.-C. Sanders, *Phys. Rev. A* **82**, 023827 (2010).
- [20] P. Fauché, S. G. Kosionis, and P. Lalanne, *Phys. Rev. B* **95**, 195418 (2017).
- [21] A. Berthelot, G. Colas des Francs, H. Varguet, J. Margueritat, R. Mascart, J.-M. Benoit, and J. Laverdant, *Nanotechnology* **30**, 015706 (2018).
- [22] A. Castellini, H. R. Jauslin, B. Rousseaux, D. Dzsojtjan, G. Colas des Francs, A. Messina, and S. Guérin, *Eur. Phys. J. D* **72**, 223 (2018).
- [23] H. Varguet, B. Rousseaux, D. Dzsojtjan, H. Jauslin, S. Guérin, and G. Colas des Francs, *J. Phys. B* **52**, 055404 (2019).
- [24] See Supplemental Material at <http://link.aps.org/supplemental/10.1103/PhysRevB.100.041115>, which includes Refs. [25–29], for details on derivation of the master equation.
- [25] D. Dzsojtjan, B. Rousseaux, H. R. Jauslin, G. Colas des Francs, C. Couteau, and S. Guérin, *Phys. Rev. A* **94**, 023818 (2016).
- [26] R. N. Annavarapu, *Ame. J. Comput. Appl. Maths.* **3**, 33 (2013).
- [27] C. Gardiner and P. Zoller, *Quantum Noise*, 3rd ed. (Springer, New York, 2004).
- [28] N. V. Vitanov and S. Stenholm, *Phys. Rev. A* **55**, 648 (1997).
- [29] H.-P. Breuer and F. Petruccione, *The Theory of Open Quantum Systems* (Oxford University Press, New York, 2002).
- [30] H. Eleuch, S. Guérin, and H. R. Jauslin, *Phys. Rev. A* **85**, 013830 (2012).
- [31] C. Navarrete-Benlloch, [arXiv:1504.05266](https://arxiv.org/abs/1504.05266).
- [32] X. Zhou, J. Wenger, F. Viscomi, L. L. Cunff, J. Béal, S. Kochtcheev, X. Yang, G. Wiederrecht, G. Colas des Francs, A. S. Bisht *et al.*, *Nano Lett.* **15**, 7458 (2015).

- [33] F. Damanet, D. Braun, and J. Martin, *Phys. Rev. A* **94**, 033838 (2016).
- [34] D. J. Bergman and M. I. Stockman, *Phys. Rev. Lett.* **90**, 027402 (2003).
- [35] M. A. Noginov, G. Zhu, A. M. Belgrave, R. Bakker, V. M. Shalaev, E. E. Narimanov, S. Stout, E. Herz, T. Suteewong, and U. Wiesner, *Nature (London)* **460**, 1110 (2009).
- [36] B. Ji, E. Giovanelli, B. Habert, P. Spinicelli, M. Nasilowski, X. Xu, N. Lequeux, J.-P. Hugonin, F. Marquier, J. Greffet *et al.*, *Nat. Nanotechnol.* **10**, 170 (2015).
- [37] P. Fauché, Ph.D. thesis, Université de Bordeaux, 2017.
- [38] S. Franke, S. Hughes, M. K. Dezfouli, P. Kristensen, K. Busch, A. Knorr, and M. Richter, *Phys. Rev. Lett.* **122**, 213901 (2019).